Directed 2D-to-3D Pattern Transfer Method for Controlled Fabrication of Topologically Complex 3D Features in Silicon

Konrad Rykaczewski,* Owen J. Hildreth, Ching P. Wong, Andrei G. Fedorov, and John Henry J. Scott

Silicon-based technologies are crucial for a variety of applications such as electronic devices,[1] photovoltaic cells,[2] optoelectronics,[3] microelectromechanical systems (MEMS),[4] and chemical and biological sensors.[5] The foundation of many of these technologies is the fabrication of micro- and nanoscale silicon features using a variety of standard wet and dry chemistry techniques that rely on etching of exposed silicon upon exposure to a reactive gas or liquid. Depending on the specific process, varied etching rates along different crystal faces result in either isotropic or strongly anisotropic etching,[6] and fabrication of 3D silicon structures is limited to relatively simple extensions of two-dimensional patterns. Metal-assisted chemical etching (MaCE) represents a fundamentally different fabrication approach in which the etching of silicon is confined to a small region surrounding metal catalyst nanoparticles or other structures that can travel in three dimensions as they etch into the silicon. Several authors recently demonstrated that MaCE based nanofabrication can exceed the capabilities of standard etching methods by making complex 3D nanostructures, such as tilted nanowires,[7,8] helical holes,[9,10] as well as cycloidal[11] and spiral[11,12] cavities with sub-10-nm feature resolutions and high aspect ratios. The key feature of the MaCE process separating it from other fabrication techniques is the possibility of arbitrarily-complex 3D motion of the catalyst particles during the etching process. Thus far, only a limited control over the 3D motion of the catalyst particles has been achieved by proper combination of particle shape, substrate crystal orientation, and etchant solution composition. For example, by varying the ratio of hydrogen peroxide (H_2O_2) and hydrofluoric acid (HF) Hildreth et al.[11] controlled the rate of in-plane rotation of metal catalyst grids, and Chern et al.[8] controlled the nanopillar tilt angle. However, it is difficult to extend this approach to simultaneously directing of 3D motion of multiple catalyst particles, such that each one follows a different trajectory. In this work, we introduce a directed MaCE process in which the 3D motion of the catalyst particles is controlled by local pinning of these structures prior to the etching. This process constrains the degrees of freedom of the metal particles during etching and results in fabrication of cavities with rotational geometry. We explore the effects of constraining simple metal catalyst structures at different locations and introduce an additional fabrication step allowing control over the rotation direction. Additionally, we show that proper design of the pinned metal catalyst structures can lead to their partial release from the silicon surface and formation of integrated 3D metal on carbon structures that are partially located within the etched silicon and partially located above the silicon surface.

In the MaCE process gold, silver, or platinum nanoparticles or patterns etch locally into silicon when exposed to a solution containing H_2O_2 and HF. Silicon etching begins with catalytic reduction of H_2O_2 on the metal surface, which creates a local cathode on the etchant side of the metal that injects holes (h^+) into the valence band of silicon, leading to a hole (h^+) rich region of silicon (Si*) surrounding the metal catalyst. The holes (h^+) are consumed at the HF/Si* interface by oxidation of Si^0 to Si^{4+} producing soluble SiF_6^{2-} and H_2SiF_6.[11,13] The etching process continues as metal nanoparticles/structures travel into the regions where the silicon was removed, forming a mobile galvanic cell as the silicon is dissolved. Depending on the etchant composition, silicon dissolution can be confined to a region in close proximity to the catalyst particle (creating high-aspect-ratio and nearly vertical protrusions into silicon) or can take place over a wide region around the catalyst particle (creating conical protrusions).[10,14]

Area-selective MaCE of silicon can be separated into two different methods. In the first method, metal nanoparticles and thin films can be directly patterned using methods such as colloidal crystal templating,[15] photo- and electron beam lithography,[11,12] microcontact imprinting,[16] superionic solid state stamping,[8] and focused ion beam induced deposition (FIBID).[17] In the second method, the etching process can be locally blocked by electron beam induced deposition (EBID) of a thin carbon layer/pattern beneath a uniform metal catalyst film.[18] The directed MaCE fabrication process combines the two above mentioned approaches. As schematically shown in **Figure 1**A–C, it consists

Dr. K. Rykaczewski
Material Measurement Laboratory
National Institute of Standards and Technology
Gaithersburg, MD 20899 — 8370, USA
E-mail: konrad.rykaczewski@nist.gov
O. J. Hildreth, Prof. C. P. Wong
School of Materials Science and Engineering
Georgia Institute of Technology
Atlanta, GA 30332, USA
Prof. A. G. Fedorov
G. W. Woodruff School of Mechanical Engineering
Georgia Institute of Technology
Atlanta, GA 30332, USA
Dr. J. H. J. Scott
Material Measurement Laboratory
Surface and Microanalysis Science Division
National Institute of Standards and Technology
Gaithersburg, MD 20899 – 8370, USA

COMMUNICATION
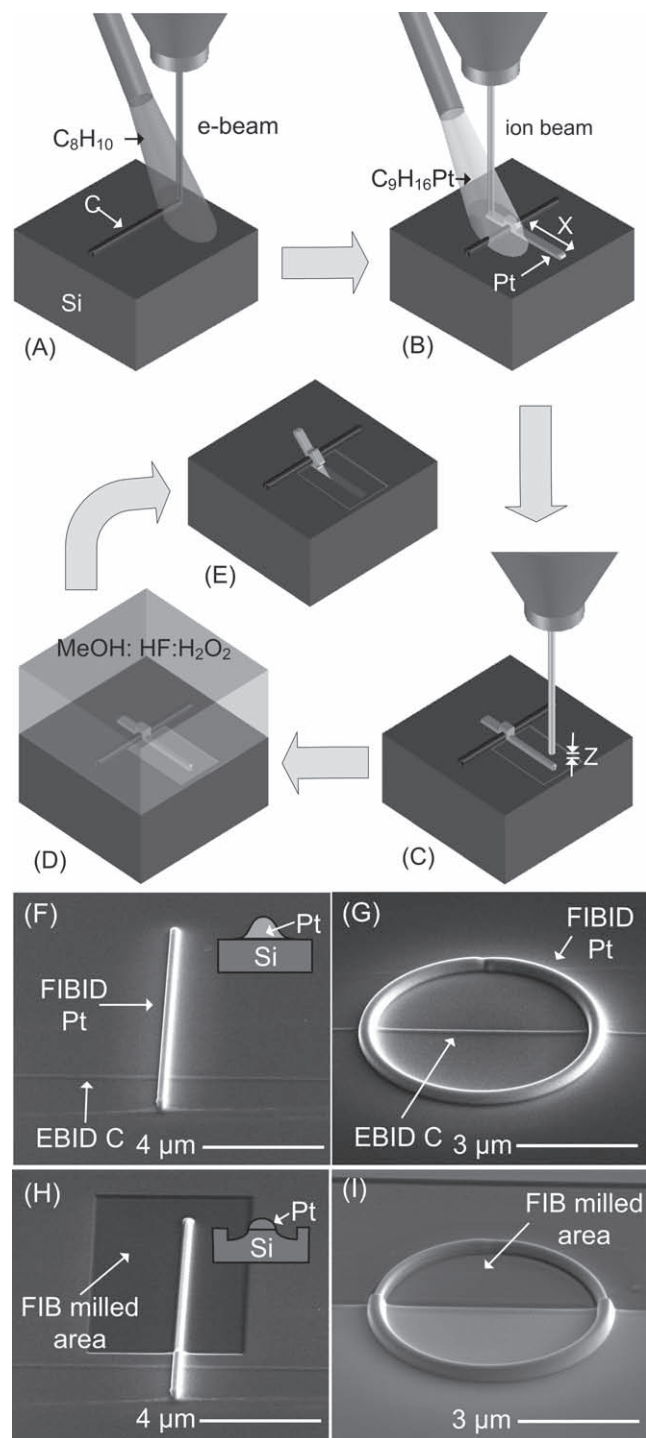
Figure 1. (A–E) Step-by-step schematic of the directed MaCE fabrication process: (A) EBID of a carbon pattern, (B) FIBID of a platinum pattern partially overlapping the carbon pattern, (C) post-deposition selective partial FIB-milling of the platinum structures and surrounding silicon, (D) etching of the sample fabricated in steps A–C in MeOH:HF:H_2O_2 solution, and (E) resulting 3D structure. (F–I) 52° SEM images of FIBID of 500-nm tall platinum structures on EBID of 100-nm tall carbon lines prior to the etching process (F,H) Pt-line-over-C-line patterns (top right side inserts show cross-sectional schematics before and after FIB-milling) and (G,I) Pt-circle-over-C-line patterns after deposition (F,G) and after selective FIB-milling of 200 nm of platinum and surrounding silicon area (H,I).

of three steps prior to etching: (1) EBID of carbon patterns, (2) FIBID of platinum patterns locally overlapping the carbon patterns, and (3) post-deposition selective FIB-milling of the platinum structures and surrounding silicon surface.

We utilize two simple geometric structures to demonstrate the capabilities of the directed MaCE fabrication process: a FIB-deposited metal catalyst line and circle over the EBID carbon line. First, we investigate etching of the platinum-over-carbon structures without the post-deposition selective FIB-milling step (Figure 1F,G). To gain insight into the process, the location of the intersection between the carbon lines and platinum structures is varied. Specifically, sets of 3 μm and 6 μm long and 300-nm tall platinum lines and 6 μm and 8 μm diameter platinum circles were etched. These metal catalyst structures intersect 100-nm tall carbon line at their mid-point, quarter way from the mid-point, and at the very end. The Pt- over-C structures were etched for short (5 and 10 min) and long (15 and 20 min) time periods.

The etched example structures shown in **Figure 2** clearly demonstrate that the carbon lines underneath the catalyst do block the etching process.[18] That is, the carbon lines locally prevent the metal catalyst structures from electrochemically interacting with and etching into the silicon. While even a 4-nm thin carbon layer is sufficient for localized blocking of the etching process,[18] in this work the carbon thickness is increased to 100 nm to increase the mechanical strength of the lines. As apparent in Figure 2, the 100-nm tall carbon lines are mechanically durable and are capable of handling significant torsional strain without failure. These properties allow the carbon lines to serve as an axis of rotation for the etching of the platinum structures resulting in removal of silicon from incomplete circular and sphere-like shell cavities. Furthermore, the etched structures shown in Figure 2 demonstrate that the adhesion between the platinum and carbon structures is significantly stronger than the adhesion between the silicon substrate and platinum deposits, resulting in numerous cases in a partial release of metal structures from the silicon and formation of integrated 3D metal-carbon-silicon structures.

Several issues arise during the etching process. As shown in Figure 2A and 2B, only a fraction (208 out of 360 or ~57%) of the Pt-over-C structures etch. Moreover, as highlighted in Figure 2F and 2G, for the structures that do etch, the direction of rotation (i.e., clockwise or counterclockwise about the etching axis) is not correlated with the position of the underlying carbon line. Of the 208 structures that did etch, 140 (~67%) rotated towards the side where the majority (Figure 2G) and 68 (~33%) where the minority (Figure 2I) of the metal structure is located. Such behavior is undesirable because it limits control over the 3D motion of the particles. Lastly, the etching process also results in formation of porous silicon in the vicinity of the platinum structures (see close-up in **Figure 3A**). While the presence of the porous silicon is potentially useful for some optical[19] or sensor applications,[20] its uncontrollable appearance is generally detrimental to the technique's practical utility.

To improve control over the metal catalyst motion and rotation direction during the etching process we introduce an additional post-deposition step consisting of selective FIB-milling of a silicon surface area containing part of the platinum structures. Selectively FIB-milled line-over-line and circle-over-line structures are shown in Figure 1H and 1I prior to the etching
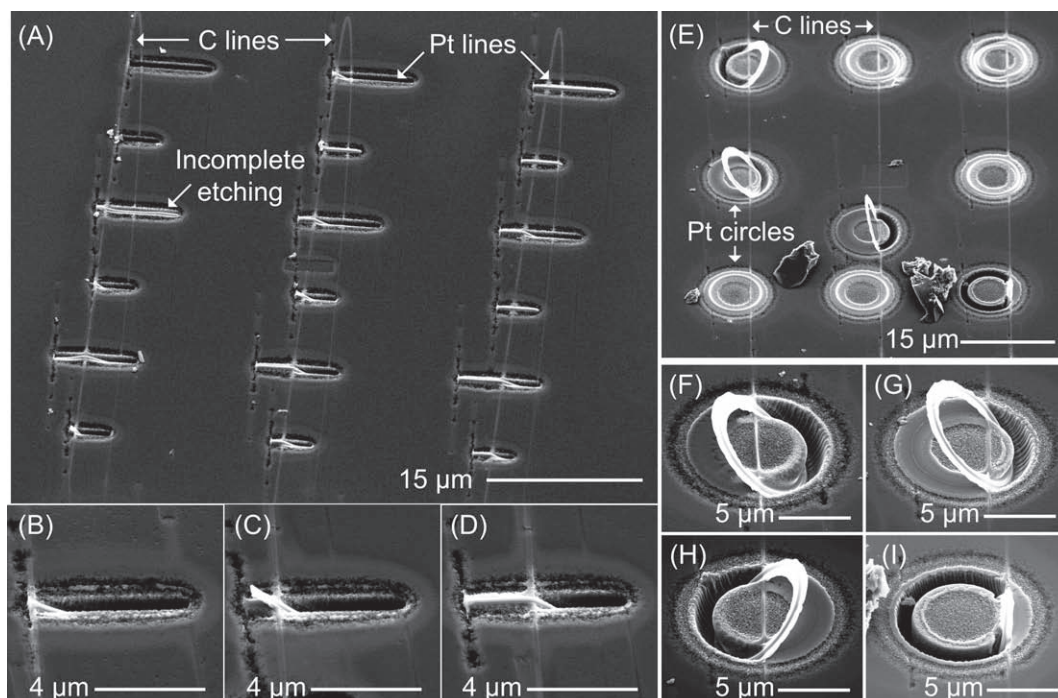
Figure 2. 45° SEM images of (A) three sets of etched 3-μm and 6-μm long, 300-nm tall platinum lines crossing over the 100-nm tall carbon line at (B) the edge point, (C) the quarter-of-the-way, and (D) the middle; (E) three sets of etched 8-μm in diameter, 300-nm tall platinum circles crossing over the 100 nm carbon line along, (F,H) the circle diameter, (G) a quarter-way off the diameter, and (I) at the point-contact to the circle circumference; line-on-line and circle-on-line structures were etched in MeOH:HF:H$_2$O$_2$ solution for 15 and 20 min, respectively.

step. Besides thinning the platinum structures, this treatment locally removes some of the bulk silicon and the undesired thin film formed near the primary platinum structures (see Figure 3D and 3K). This platinum- and carbon-containing film forms during the EBID and FIBID processes due to adsorbed precursor and hydrocarbon contamination decomposition by non-localized secondary electrons generated by back- and side-scattered electrons and ions.[21] The film can extend several micrometers away from the primary structure and can fill in the inner area of the platinum circles (see Figure 3G).

Examples of partially FIB-milled and etched structures are shown in Figure 3. Several improvements are observed over the structures produced by etching without the selective FIB-milling treatment. First, the etching rate is significantly increased. After 1 min of etching the FIB-treated areas, the depth of etch is comparable to that obtained after the long etching period of 15–20 min without the FIB pre-treatment. Second, 95 out of the 120 (~80%) fabricated test structures etch and 95 out of 95 (100%) rotate towards the side that underwent the partial FIB-milling treatment (see example structure sets in Figure 3A and 3B). After the short etching time (30 s) only 18 of the 40 (~45%) of the structures that etched are released from Si surfaces while after the long etching time (60 s) 51 out of 55 (~91%) of the structures are released from Si surface. To provide a conservative estimate of the etch yield, metal structures that have returned to their original (horizontally oriented) shape from the partially deformed state and partially cover up the etched-out cavities are counted as a failed etch. Close-up images of the etched line-over-line (Figure 3C–F) and circle-over-line (Figure 3G–J) structures

clearly demonstrate the high degree of control over the rotation direction. These images also demonstrate the improved resolution (the width decreased from previous ~600–1000 nm to ~300–500 nm) of the etched trenches and a significant decrease in formation of the porous silicon within the areas milled by the FIB. In addition, Figure 3K shows that etching of the circle-over-line structures for 2 min can result in 180° rotation of the platinum circle around the carbon line and removal of silicon from half-spherical shell cavities. Accidental dislocation of the released silicon piece and metal catalyst structure, which likely occurred during the water rinsing step, clearly reveals the rotational nature of the etched-out cavity. The structures shown in Figure 3 were FIB-milled from height of 500 nm to 300–350 nm. FIB-milling beyond this thickness is undesirable, because it results in an increased flexibility of the metal structures and corresponding increase in their deformation during the etching step.

The likely mechanism causing the preferential rotation towards the FIB-milled side is a locally increased etch rate due to a decreased width of metal lines and exposure of an additional area of silicon below the platinum structures (see schematic in Figure 1H). The imbalance between the etching rates induces an asymmetry in the mechanical forces on the Pt structure, thus causing a preferential rotation about the carbon line axis in the direction of the milled/thinned side. Since an increase in the etch time significantly increases the fraction of the Pt structures released from Si surface, the release process is likely to occur suddenly when a threshold imbalance between the mechanical forces due to bending and adhesion is reached. After their release, the deformed metal structures (such as the long bent lines in
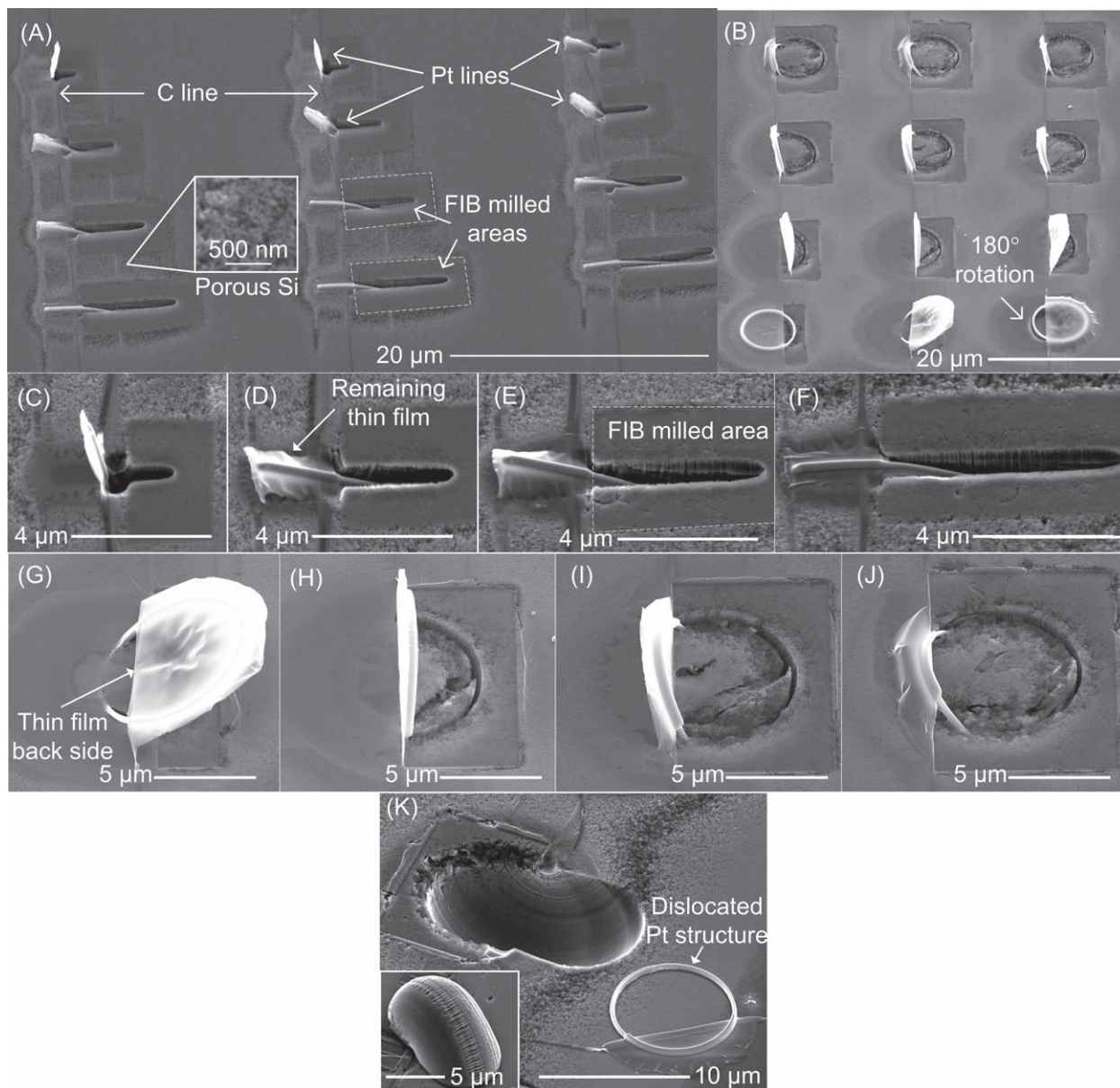
Figure 3. 45° SEM images of (A) three sets of etched 450-nm tall platinum lines that cross the underlying 100-nm tall carbon lines at 2 μm from left edge and are selectively FIB-milled on the right side (100 nm milling depth), (B) three sets of etched 8-μm in diameter and 500-nm tall platinum circles, (C–F) close-up of example of the etched (C) 4 μm, (D) 6 μm, (E) 8 μm, and (F) 10 μm platinum-line-over-carbon-line structures; (G–J) close-up of rotated upon etching platinum-circle-over-carbon-line structures that cross the underlying 100-nm tall carbon lines (J) directly at, (I) quarter, (H) half, and (G) three-quarter diameter away from the left edge and are selectively FIB-milled (200 nm milling depth) on the right side; (K) example of 8-μm platinum circle with carbon line offset by a quarter of circle diameter from the left edge, insert in the left lower corner shows the etched out half-spherical silicon structure removed from bulk silicon during etching. The structures were etched in MeOH:HF:H_2O_2 solution for (A–J) 1 min and (K) 2 min.

Figure 3A and 3F) can return to their original shape due to bending stress relaxation, while the carbon line continues to twist due to etching of the submerge part of the catalyst structure.

In summary, in this work we introduce a new process allowing control of the rotation of metal catalyst nanostructures during the MaCE etching process, resulting in etching of complex 3D patterns in bulk silicon. The method is based on constraining the degrees of freedom for motion of metal catalyst structures by local pinning prior to etching. This is accomplished using

EBID carbon lines underneath the metal catalyst structure. As demonstrated by MaCE etching of Pt-line-over-C-line and Pt-circle-over-C-line structures, the underlying carbon line acts as fulcrum for rotation of the platinum structures. Undesired effects such as low etch yield, limited control over the rotation direction, poor resolution of pattern transfer, and porous silicon formation associated with conventional implementation of MaCE etching process are significantly improved by selective post-deposition FIB-milling of the platinum structures

and surrounding silicon surface. As in the case of self-assembly methods relying on stress induced curvature, the basic principle introduced in this work (i.e., controlling 3D etching motion of metal catalyst nanostructures/patterns by their local pinning using catalytically inactive anchors placed underneath of the catalyst structure) should be extendable to other material systems and etching chemistries. While initially producing relatively simple geometries,[22] recent achievements in material systems and fabrication method have pushed the capabilities of stress-induced self-assembly fabrication to wafer scale production of structures, such as multimaterial-patterned cylinders, cubes, polyhedrons, and other complex 3D structures on micro- and nanoscale.[23] With equivalent refinements, the fabrication method introduced in this work should be capable of producing a rich variety of complicated etch patterns in 3D, including formation of suspended structures and potentially be applicable to production of 3D micro- and nanodevices on a wafer scale.

Experimental Section

FIBID Platinum and EBID carbon structures: All samples are prepared on a single-side-polished p-type (8 Ωcm^{-1} to 12 Ωcm^{-1}) single crystal (100) silicon wafer cleaned using dilute HF (1:10) for 30 s. All structures are fabricated using an FEI Nova Nanolab 600 Dual Beam instrument (certain commercial equipment, instruments, and materials are identified in this publication to adequately specify the experimental procedure. Such identification in no way implies approval, recommendation, or endorsement by NIST, nor does it imply that the equipment, instruments, or materials identified are necessarily the best available for the purpose). The 100-nm tall EBID carbon structures are fabricated using naphthalene ($C_{10}H_8$) gas precursor, electron beam energy of 2 keV and current of 53 pA, and dwell time of 200 ns. The 250–500-nm tall FIBID Pt structures are fabricated using C_9H_{16}Pt gas precursor, ion beam energy of 30 keV, current of 48 pA, and dwell time of 200 ns. The structures are subsequently FIB-milled to depths specified in the article with ion beam energy of 30 keV, current of 48 pA, and dwell time of 1 µs.

MaCE: All structures are etched in a mixture of 16 mL of HF (Aldrich, 49%), 4.8 mL of H_2O_2 (Aldrich, 30%), and 6.8 mL of MeOH for a period of 0.5, 1, 2, 5, 10, 15, and 20 min at room temperature. A drop of the etchant solution is dispensed onto a sample using a pipette. After etching, the samples are thoroughly rinsed in DI water and dried with nitrogen gas. Etched structures are imaged using an FEI Quanta 200 FEG ESEM at 5 keV electron beam energy and spot size 3.

Acknowledgements

[1] T. Ito, T. Yamada, Y. Inao, T. Yamaguchi, N. Mizutani, R. Kuroda, *Appl. Phys. Lett.* **2006**, *89*, 3.

[2] S. Koynov, M. S. Brandt, M. Stutzmann, *Appl. Phys. Lett.* **2006**, *88*, 3.

[3] S. M. Weiss, M. Haurylau, P. M. Fauchet, *Opt. Mater.* **2005**, *27*, 740.

[4] Y. Ben, Y. Gianchandani, G. Peterson, P. Bergsrom, G. Li, D. Plummer, A. Borboni, L. Ofdahl, C. Sobhan, E. Muntz, *MEMS Applications*, CRC, Boca Ranton, FL **2005**.

[5] a) L. Brus, *J. Phys. Chem.* **1994**, *98*, 3575; b) V. S. Y. Lin, K. Motesharei, K. P. S. Dancil, M. J. Sailor, M. R. Ghadiri, *Science* **1997**, *278*, 840; c) M. J. Sailor, E. J. Lee, *Adv. Mater.* **1997**, *9*, 783.

[6] M. J. Madou, *Fundametals of microfabrication: The science of miniaturization,* CRC, New York **2002**.

[7] K. Peng, A. Lu, R. Zhang, S. T. Lee, *Adv. Funct. Mater.* **2008**, *18*, 3026.

[8] W. Chern, K. Hsu, I. S. Chun, B. P. d. Azeredo, N. Ahmed, K.-H. Kim, J.-m. Zuo, N. Fang, P. Ferreira, X. Li, *Nano Lett.* **2010**, *10*, 1582.

[9] a) K. Tsujino, M. Matsumura, *Adv. Mater.* **2005**, *17*, 1045; b) K. Tsujino, M. Matsumura, *Electrochem. Solid-State Lett.* **2005**, *8*, C193.

[10] K. Tsujino, M. Matsumura, *Electrochim. Acta* **2007**, *53*, 28.

[11] O. J. Hildreth, W. Lin, C. P. Wong, *ACS Nano* **2009**, *12*, 4033.

[12] I. S. Chun, E. K. Chow, X. L. Li, *Appl. Phys. Lett.* **2008**, *92*, 3.

[13] P. Gorostiza, R. Diaz, M. A. Kulandainathan, F. Sanz, J. R. Morante, *J. Electroanal. Chem.* **1999**, *469*, 48.

[14] C. Chartier, S. Bastide, C. Levy-Clement, *Electrochim. Acta* **2008**, *53*, 5509.

[15] H. Asoh, F. Arai, S. Ono, *Electrochem. Commun.* **2007**, *9*, 535; H. Asoh, F. Arai, K. Uchibori, S. Ono, *Appl. Phys. Express* **2008**, *1*, 3.

[16] Y. Harada, X. L. Li, P. W. Bohn, R. G. Nuzzo, *J. Am. Chem. Soc.* **2001**, *123*, 8709.

[17] S. Chattopadhyay, P. W. Bohn, *J. Appl. Phys.* **2004**, *96*, 6888.

[18] K. Rykaczewski, O. J. Hildreth, D. Kulkarni, M. R. Henry, S. K. Kim, C. P. Wong, V. V. Tsukruk, A. G. Fedorov, *ACS Appl. Mater. Interfaces* **2010**, *2*, 969.

[19] X. Li, P. W. Bohn, *Appl. Phys. Lett.* **2000**, *77*, 2572.

[20] P. Kui-Qing, W. Xin, L. Shuit-Tong, *Appl. Phys. Lett.* **2009**, *95*, 243112.

[21] a) K. Rykaczewski, W. B. White, A. G. Fedorov, *J. Appl. Phys.* **2007**, *101*, 054307; b) K. Rykaczewski, A. Marshall, W. B. White, A. G. Fedorov, *Ultramicroscopy* **2008**, *108*, 989; c) I. Utke, P. Hoffmann, J. Melngailis, *J. Vac. Sci. Technol. B* **2008**, *26*, 1197.

[22] a) V. Y. Prinz, V. A. Seleznev, A. K. Gutakovsky, A. V. Chehovskiy, V. V. Preobrazhenskii, M. A. Putyato, T. A. Gavrilova, *Physica E: Low Dim. Sys. Nanostruct.* **2000**, *6*, 828; b) O.G. Schmidt, N. Schmarje, C. Deneke, C. Müller, N.Y. Jin-Phillipp, *Adv. Mater.* **2001**, *13*, 756; c) O. G. Schmidt, K. Eberl, *Nature* **2001**, *410*, 168; d) M. Boncheva, G. M. Whitesides, *Adv. Mater.* **2005**, *17*, 553; e) W.J. Arora, A. J. Nichol, H. I. Smith, G. Barbastathis, *Appl. Phys. Lett.* **2006**, *88*, 3.

[23] a) P. Tyagi, N. Bassik, T. G. Leong, C. Jeong-Hyun, B. R. Benson, D. H. Gracias, *J. Microelectromech. Syst.* **2009**, *18*, 784; b) P. Stellman, T. Buchner, W. J. Arora, G. Barbastathis, *J. Microelectromech. Syst.* **2007**, *16*, 932; c) N. Bassik, G. M. Stern, M. Jamal, D. H. Gracias, *Adv. Mater.* **2008**, *20*, 4760; d) H. J. In, S. Kumar, Y. Shao-Horn, G. Barbastathis, *Appl.Phys. Lett.* **2006**, *88*, 3; e) J. H. Cho, T. James, D. H. Gracias, *Adv. Mater.* **2010**, *22*, 2320; f) J.-H. Cho, D. H. Gracias, *Nano Lett.* **2009**, *9*, 4049.